Robotics and Autonomous Systems 150 (2022) 103995

Contents lists available at ScienceDirect

Robotics and Autonomous Systems

journal homepage: www.elsevier.com/locate/robot

Hovering control of an underwater robot with tilting thrusters using the decomposition and compensation method based on a redundant actuation model

Jeongae Bak [a], Yecheol Moon [b], Jongwon Kim [c], Santhakumar Mohan [d], TaeWon Seo [b,*], Sangrok Jin [e,*]

[a] Department of Robotics and Mechatronics, Korea Institute of Machinery and Materials, Daejeon, 34103, Republic of Korea
[b] Department of Mechanical Eng., Hanyang Univ., Seoul, 04762, Republic of Korea
[c] School of Mechanical and Aerospace Eng., Seoul Nat'l Univ., Seoul, 08826, Republic of Korea
[d] Discipline of Mechanical Eng. Indian Institute of Technology, Palakkad, India
[e] School of Mechanical Eng., Pusan Nat'l Univ., Pusan, 46241, Republic of Korea

ARTICLE INFO

Article history:
Received 25 May 2020
Received in revised form 20 December 2021
Accepted 22 December 2021
Available online 4 January 2022

Keywords:
Hovering control
Underwater robot
Tilting thruster
Redundant tilting mechanism
Empirical model compensation

ABSTRACT

Six-degree-of-freedom (6-DOF) hovering control is important for underwater robots to perform various tasks. Our previous underwater robot study, which used tilting thrusters, could not control 6-DOF motion simultaneously owing to several mechanical and control problems. In this study, we developed a new robot with tilting thrusters and improved 6-DOF hovering performance. The maneuverability of the robot was evaluated by analyzing the force and moment of the thrust vector. Based on this, a redundant tilting mechanism without constraints was designed to solve structural problems. A proportional–integral–derivative (PID)-based control design using the decomposition and compensation method (PID-DC) that is appropriate for this mechanism, was derived. The decomposition method was used to overcome the nonlinearity of the thrust vector caused by the tilting mechanism, and the null-space projection technique was applied to minimize the thrust force and avoid the boundary of the tilting angle. A compensator based on the empirical model of the tilting thruster transferred the control input to the system with regulation. Simulation and experimental results verified the validity of the controller for the 6-DOF hovering motion of the robot, and the hovering performance was significantly improved. Furthermore, the stability of the hovering performance under tidal currents was demonstrated through disturbance experiments.

1. Introduction

In hazardous underwater environments, divers perform inefficient and often dangerous tasks. Several underwater robots have been developed to work efficiently in water. For an underwater robot to work well, it is essential for it to perform a six-degree-of-freedom (6-DOF) hovering motion [1].

Underwater robots with fixed thrusters have been widely developed because thrusters are the main power source for such robots [2–4]. By reducing the number of thrusters, the robots' size, weight, and power consumption can be reduced. Accordingly, tilting and thrust-vectoring mechanisms have been widely investigated owing to their advantages [5–7]. In addition, it is possible to compensate for the disturbance by concentrating the thrust force of a constant disturbance in a certain direction.

ODYSSEY IV [8] was equipped with rotating thruster units and a thruster layout, two vectored side thrusters, and two fixed cross-body thrusters, which enabled 4-DOF control. Otohime [9], PICASSO [10], SeaBird [11], and AUV from Ottawa University [12] are the underwater robots with tilting thrusters that are similar to those used in ODYSSEY IV. JAMSTEC developed an underwater robot called Otohime with two azimuth thrusters, two vertical rudders, and two horizontal rudders. JAMSTEC also designed PICASSO, which has two lateral thrusters at 120° and a vertical thruster for highly maneuverable cruising. The glider type of small AUV, the SeaBird, was equipped with two thrusters that were rotated by each servo motor. Ottawa University developed an AUV with two vectored thrusters and 5-DOF—horizontal and

* Corresponding authors.
E-mail addresses: taewonseo@hanyang.ac.kr (T. Seo), rokjin17@pusan.ac.kr (S. Jin).

https://doi.org/10.1016/j.robot.2021.103995
0921-8890/

Nomenclature

η	Position and orientation vector in the earth-fixed frame
v	Linear and angular velocity in the body frame
$\mathbf{J}$	Jacobian matrix
$\mathbf{M}$	Inertial matrix
$\mathbf{C}$	Coriolis matrix
$\mathbf{D}$	Damping matrix
$\mathbf{K}_p$	Proportional gain matrix
$\mathbf{K}_i$	Integral gain matrix
$\mathbf{K}_d$	Differential gain matrix
$g(\eta)$	Gravitational force and buoyant force
τ	Thrust vector
f_i	Force of ith thrust
θ_i	Tilting angle of ith thrust
Ω	Input RPM of thruster's propeller
q	Control input
z	Additional command
e	Position and orientation error
Δt	Control period
$H(\theta)$	Function for tilting angle limitation
k_H	Gain for $H(\theta)$
k_h	Gain for null-space projection

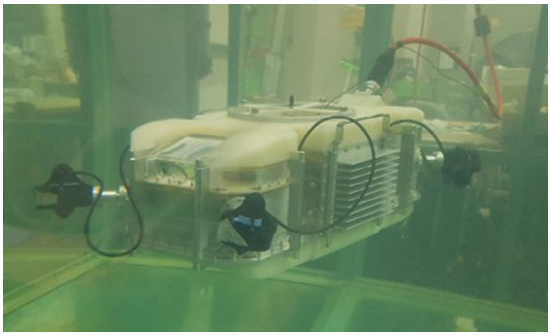

Fig. 1. Underwater robot with redundant tilting thrusters: AURORA.

vertical movements, and rotations around the x-, y-, and z-axes. Moreover, the spherical underwater robot (SUR III) from Kagawa University has four thrusters that rotate on two axes and implement 4-DOF movements [13]. Most of these robots cannot implement a 6-DOF hovering motion. While some of them have performed field tests, most were only inspected in water without performing tasks.

A tilt-thrusting underwater robot (TTURT) [14] is designed to allow 6-DOF motion control for various underwater tasks such as turning the valves of underwater structures [15] and capturing starfish [16] using a manipulator. The most important feature of TTURT is that it has a tilting mechanism with constraints. Two tilting thrusters make one set, and the front and rear of the robot body have one set each. Each set of thrusters is simultaneously tilted by a motor. However, this tilting mechanism makes the thrust vector nonlinear, and simple linear control cannot be easily applied. Furthermore, constraints are caused by a set of thrusters that are simultaneously forced to rotate at the same angle. Another limitation is the speed saturation of the actuators, which cannot keep up with the control input from the controller. Owing to these constraints, the mechanism has structural problems that prevent the robot from maintaining a 6-DOF motion. Jin [17] and Bak [18] have simulated 6-DOF hovering motion control, but it could not be applied because they had not considered practicality.

TTURT is controlled by a switching PD control, which was designed to select one of the two subsystems based on horizontal and vertical modes. Each 3-DOF mode was controlled separately when all four tilting angles were 0° or 90°. Because of this, the robot not only has an unstable hovering motion but also the potential to diverge when there is a large disturbance, such as ocean currents. A switching PD-SMC has been applied, but it also uses only two discrete tilting angles (0° and 90°), and not continuous tilting. Consequently, the robot still has trouble with vibrations in the steady state [14,19].

We propose an underwater robot with tilting thrusters for redundant actuation (AURORA), as shown in Fig. 1. For achieving effective hovering control, AURORA was upgraded to a new version of TTURT, and the tilting mechanism in the robot box was redesigned. The robot platform has four tilting thrusters in vertex positions based on a rectangular-shaped mainframe. The thrusters can be tilted to achieve a 6-DOF motion depending on their configuration. The robot also has a docking mechanism designed on the platform-module concept for various underwater tasks, and various modules can be attached to module the attachment point of the robot.

For a more stable 6-DOF hovering motion, the robot needs a suitable control method for the proposed tilting mechanism. Therefore, a new controller adapted to AURORA was designed by reflecting the model of the actual tilting thruster and finding a practical solution using the redundancy. The nonlinear force input term is divided into thrust forces and thrust angles by decomposition in the horizontal and vertical directions. An algorithm, which is determined by a pseudo-inverse and null-space projected gradient method, is added to this controller, and the solution is found by minimizing the thrust force and avoiding the bound of the tilting angles. The final control input is derived from a compensator based on an empirical model of the tilting mechanism.

The main contributions of this paper are as follows.
(1) Designing a redundant tilting mechanism without constraints to solve the structural problem,
(2) Developing a PID-based control design using the decomposition and compensation method, which is appropriate to this tilting mechanism,
(3) Verifying the validity of this controller for 6-DOF hovering motion of the robot by simulation and experimentation.

The remainder of this paper is organized as follows. In Section 2, the redundant tilting mechanism of AURORA is introduced. We analyzed the structural problems of the tilting mechanism and conducted experiments to obtain an empirical model for it. Section 3 describes the design of the proposed control, along with a stability analysis. The simulation and experimental results are presented in Sections 4 and 5. These results verify the hovering ability of the robot and confirm that its performance is improved compared to other controls. Finally, conclusions are summarized in Section 6.

2. Redundant tilting mechanism

AURORA has a redundant tilting mechanism, i.e., four tilting thrusters that can be rotated independently in the vertex positions based on a rectangular-shaped mainframe, as shown in Fig. 2(a). The thrust vector for generating the force is presented in Eq. (1), and the thrust force and moment vector τ are determined from the position and direction of the thrusters, as shown

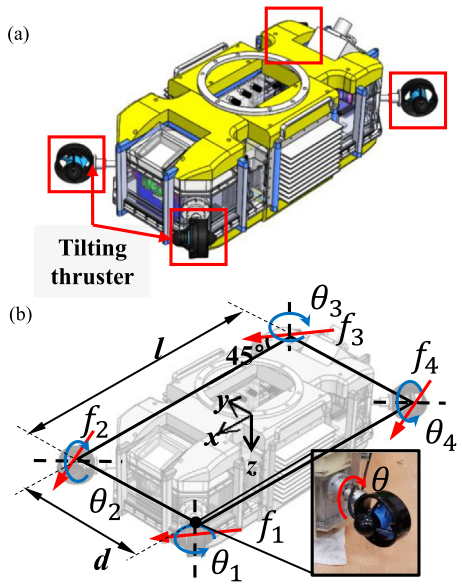

Fig. 2. (a) Redundant tilting mechanism with four tilting thrusters. (b) Configuration of thrust vector.

Table 1
Circularity of force and moment area.

	F_y–F_z	M_y–M_z	F_x–F_z	M_x–M_z
Previous tilting mechanism	0.41	0.42	0.10	0.09
Redundant tilting mechanism	0.93	0.97	0.24	0.11

in Fig. 2(b)

$$\tau = \begin{bmatrix} \frac{1}{\sqrt{2}}(f_1\cos\theta_1 + f_2\cos\theta_2 + f_3\cos\theta_3 + f_4\cos\theta_4) \\ \frac{1}{\sqrt{2}}(f_1\cos\theta_1 - f_2\cos\theta_2 + f_3\cos\theta_3 - f_4\cos\theta_4) \\ -f_1\sin\theta_1 - f_2\sin\theta_2 - f_3\sin\theta_3 - f_4\sin\theta_4 \\ \frac{d}{2}(f_1\sin\theta_1 - f_2\sin\theta_2 - f_3\sin\theta_3 + f_4\sin\theta_4) \\ \frac{l}{2}(f_1\sin\theta_1 + f_2\sin\theta_2 - f_3\sin\theta_3 - f_4\sin\theta_4) \\ \frac{l+d}{2\sqrt{2}}(f_1\cos\theta_1 - f_2\cos\theta_2 - f_3\cos\theta_3 + f_4\cos\theta_4) \end{bmatrix} \quad (1)$$

where f_1, f_2, f_3, and f_4 are the thrust forces generated by each thruster, θ_1 and θ_2 are the left and right front tilting angles, θ_3 and θ_4 are the right and left rear tilting angles, and l and d are the length and width of the robot platform, respectively.

2.1. Analysis of the system structure

A previous study proposed TTURT, and the tilting mechanism inside this robot is shown in Fig. 3(a). The robot's thrusters are connected to the servo motor for rotation, and two thrusters are connected to one tilting motor by a gear. Therefore, the two front thrusters rotate simultaneously, and the two rear thrusters are also driven. Owing to these constraints, the mechanism has structural problems. In this structure, it is difficult for the robot to maintain a 6-DOF motion [17].

However, the newly designed redundant tilting mechanism shown in Fig. 3(b) has a total of eight actuators, and each thruster is connected to one tilting motor. Therefore, each tilting thruster is independently rotatable and has none of the previous constraints.

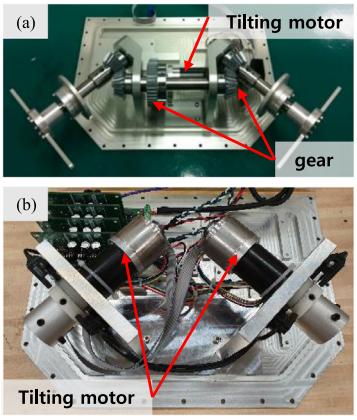

Fig. 3. (a) Previous tilting mechanism with constraints. (b) Redundant tilting mechanism.

The forces and moments that can be derived from the tilting mechanism consisting of the four tilting thrusters, are the main elements of the robot converging to the desired position and posture. These were analyzed assuming that the thrust force of each thruster was −5 N to 5 N, and the tilting angle was −90° to 90°. In Fig. 4, forces and moments from the previous tilting mechanism with constraints (i.e., six actuators) are represented in sky blue, whereas forces and moments from the mechanism without constraints are described in blue. An unconstrained mechanism is assumed to have eight actuators. It can be seen that the force and moment area that can be produced by the six actuators are much smaller than those produced by the eight actuators.

The definition of circularity defined by Cox is given as follows [20].

$$Circularity = \frac{4\pi A}{p^2} \quad (2)$$

where A is the area and p is the perimeter. The circularity ranges from 0 to 1, and the closer it is to 1, the more circular it is. The analysis results are described in a two-dimensional plane for easier viewing. The circularity in this area was calculated and is presented in Table 1. The areas of the F_x–F_y and M_x–M_y planes are determined by the shape to which the thrusters are attached. Therefore, they were ignored because their areas were not circular. In all cases, the blue area is wider and more evenly distributed than that in sky blue, meaning that the mechanism without constraints can generate more uniform forces and moments in all directions. This means that the movement of the robot with a mechanism without constraints can be controlled more stably. In particular, the force area in the F_y–F_z plane and the moment area in the M_y–M_z direction are small. Therefore, it is challenging to produce the force and moment in that direction. It turns out that no-solution areas exist mathematically, and they are unstable as mechanical structures.

2.2. Modeling of tilting mechanism

A model of a tilting mechanism consisting of thrusters and tilting motors was obtained through experiments in water. The well-known thrust theory is as follows [21].

$$F = \rho D^4 K\,|\Omega|\,\Omega \quad (3)$$

where F is the thrust force, ρ is the water density, D is the propeller diameter, K is a coefficient, and Ω is the propeller shaft speed. Coefficient K is not constant; rather, it is a function of the propeller shaft velocity, internal flow velocity, and diameter of

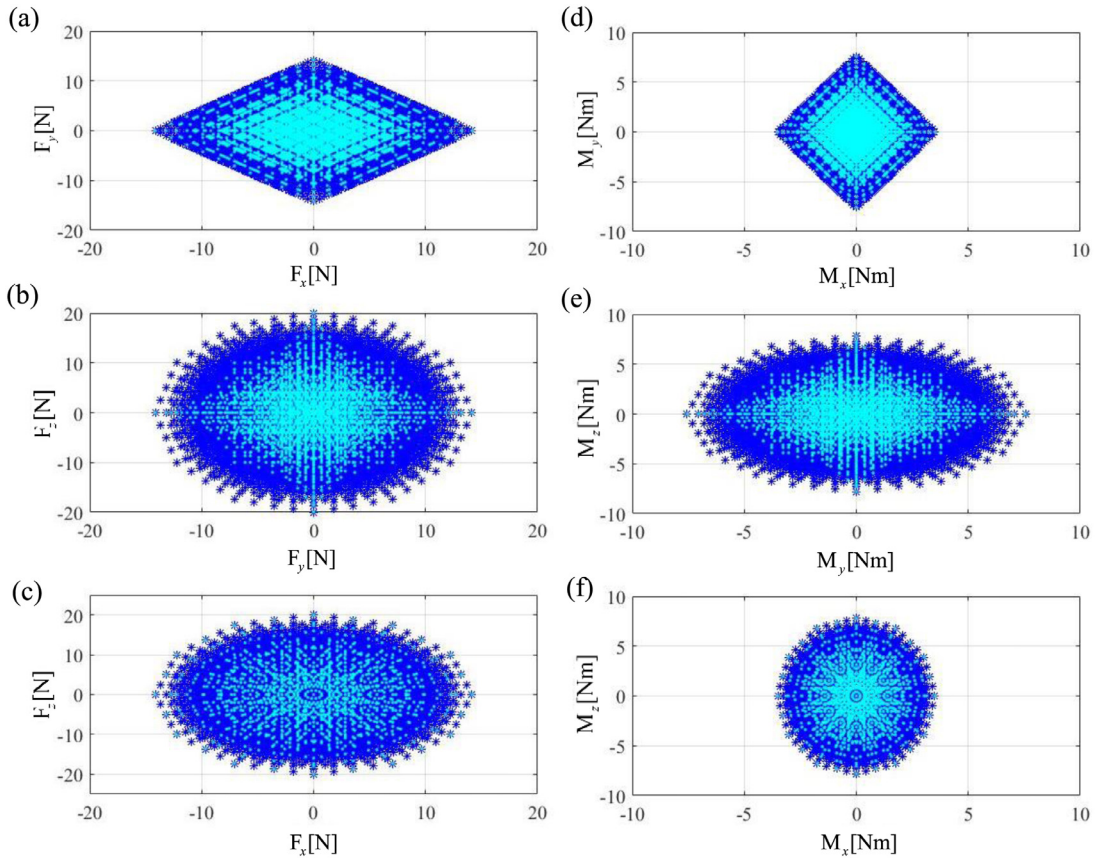

Fig. 4. Analysis of force and moment from tilting thrusters in 2-D dimension. Constrained mechanism data is denoted as sky blue, and unconstrained mechanism is presented a blue; force area in (a) F_x–F_y plane; (b) F_y–F_z plane; (c) F_x–F_z plane; moment area in (d) M_x–M_y plane; (e) M_y–M_z plane; (f) M_x–M_z plane. . (For interpretation of the references to color in this figure legend, the reader is referred to the web version of this article.)

the propeller. This coefficient is obtained experimentally in many cases owing to the complexity of the function.

Thrust force is a function of the propeller shaft speed, as shown in Eq. (3). However, it is difficult to calculate the thrust force because many thrusters do not have encoders, and the non-contact tachometer is not accurate when the object operates in a water tank [22]. Therefore, the relationship between the thrust force and input revolutions per minute (RPM) was empirically modeled. The empirical thrust force model for the input RPM in the steady state was obtained by measuring the reaction force using the force sensor. The relationship between the thrust force and input RPM is described as a quadratic equation with a dead zone, as shown in Fig. 5(a). The empirical expression for the thrust force in the steady state is similar to the general formula and is derived as follows.

$$\begin{aligned} F_{ss} &= 3.96 \times 10^{-6}\Omega^2 \quad for\ \Omega > 300\ and \\ &= 3.30 \times 10^{-6}\Omega^2 \quad for\ \Omega < -300, \end{aligned} \tag{4}$$

where F_{ss} is the thrust force in the steady state, and Ω is the input RPM. The dead zone of the thruster was ± 300 rpm.

An input RPM generates a thrust force with a delay because of the electromechanical dynamics of the motor, and the hydrodynamics of fluid propagation. The thrust force in the transient state was also measured, and this equation for the actual thruster model was obtained.

$$\begin{aligned} \Omega_{n+1} &= \Omega_n \qquad for\ \ \Omega_n = \Omega_d \\ &= \Omega_n + 5900t_s \ for\ \ \Omega_n < \Omega_d \\ &= \Omega_n - 5900t_s \ \ for\ \ \Omega_n > \Omega_d \end{aligned} \tag{5}$$

where Ω_d is the original desired input RPM from the controller, Ω_n is the nth of the RPM of the thruster, Ω_{n+1} is the next step of the thruster RPM, and t_s is the time. Fig. 5(b) shows the experimental results of the step response for the empirical model and the simulation plot of the obtained model.

There is also a delay in driving the tilting motor because it must have an acceleration and deceleration time. Similarly, the tilting angles in the transient state were measured, and an equation for the actual tilting motor model was obtained.

$$\begin{aligned} \theta_{n+1} &= \theta_n \qquad for\ \ \theta_n = \theta_d \\ &= \theta_n + 670t_s \ for\ \ \theta_n < \theta_d \\ &= \theta_n - 670t_s \ \ for\ \ \theta_n > \theta_d \end{aligned} \tag{6}$$

where θ_d is the original desired input tilting angle from the controller, θ_n is the nth of the angles of the tilting motor, Ω_{n+1} is the next step of the tilting angle, and t_s is the time. The experimental results are shown in Fig. 5(c), and they represent the empirical model of the actual tilting motor.

3. Control design

Proportional integral and derivative control (PID control) is the most commonly used control technique. The controller is simple in structure, relatively easy to adjust parameters, and has excellent control performance. In actual industrial sites, reliable PID controllers are still widely used despite the rapid advancement of modern control theory [23,24].

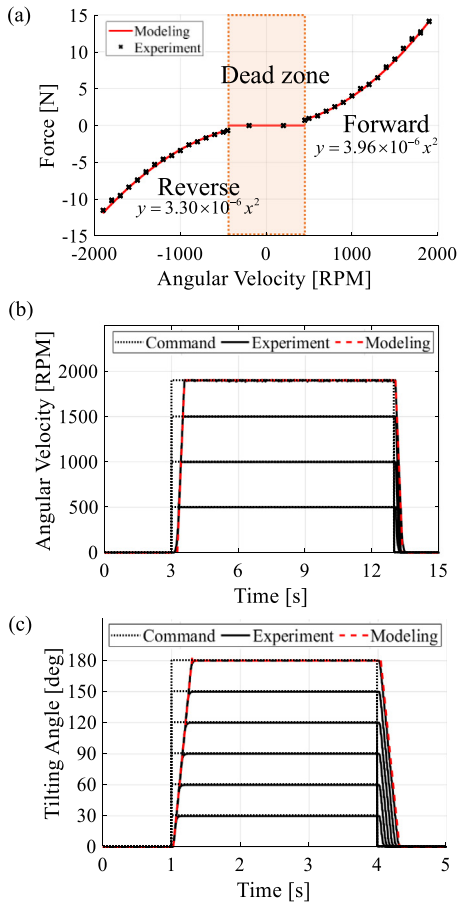

Fig. 5. (a) Thruster force versus input RPM in the steady state. (b) Step response of the thruster RPM in the transient state. (c) Step response of the tilting motor, experimental results and empirical model of the thruster and tilting motor.

AURORA also uses a PID-type controller. However, it is challenging to control the robot because of the nonlinearity of the thrust vector and the limitations of the tilting thruster when used practically. Therefore, the PID-DC controller is designed to offer robust control of the 6-DOF motion, as shown in Fig. 6. The forces and moments derived from it are properly adjusted by a vector decomposition method and a compensator based on the tilting mechanism model.

First, the thrust vector to achieve the desired position and orientation can be obtained through a simple PID control. This derived thrust is converted to thruster forces and tilting angles using the vector decomposition technique. In the next step, an algorithm to find a more practical solution using a null-space is applied to the controller. Finally, a compensator reflecting the actual tilting thruster model is added to solve the saturation of the actuator speed.

3.1. Decomposition of the thrust vector

The tilting mechanism has a nonlinear model because of the tilting angle. To overcome the nonlinearity of the thrust vector, the thrust vector, τ, is decomposed into horizontal and vertical components as follows [18].

$$\tau = \mathbf{A}q \tag{7}$$

where

$$\mathbf{A} = \begin{bmatrix} 0 & 0 & 0 & 0 & \frac{1}{\sqrt{2}} & \frac{1}{\sqrt{2}} & \frac{1}{\sqrt{2}} & \frac{1}{\sqrt{2}} \\ 0 & 0 & 0 & 0 & \frac{1}{\sqrt{2}} & -\frac{1}{\sqrt{2}} & \frac{1}{\sqrt{2}} & -\frac{1}{\sqrt{2}} \\ -1 & -1 & -1 & -1 & 0 & 0 & 0 & 0 \\ \frac{d}{2} & -\frac{d}{2} & -\frac{d}{2} & \frac{d}{2} & 0 & 0 & 0 & 0 \\ \frac{l}{2} & \frac{l}{2} & -\frac{l}{2} & -\frac{l}{2} & 0 & 0 & 0 & 0 \\ 0 & 0 & 0 & 0 & \frac{l+d}{2\sqrt{2}} & -\frac{l+d}{2\sqrt{2}} & -\frac{l+d}{2\sqrt{2}} & \frac{l+d}{2\sqrt{2}} \end{bmatrix},$$

$$q = \begin{bmatrix} f_1 \sin\theta_1 \\ f_2 \sin\theta_2 \\ f_3 \sin\theta_3 \\ f_4 \sin\theta_4 \\ f_1 \cos\theta_1 \\ f_2 \cos\theta_2 \\ f_3 \cos\theta_3 \\ f_4 \cos\theta_4 \end{bmatrix}.$$

The complex thrust vector is decomposed into a constant matrix $\mathbf{A} \in \Re^{6\times8}$ and an input column vector $q \in \Re^8$. Solving for q, we get

$$q = \mathbf{A}^+\tau \tag{8}$$

where the superscript $+$ is the Moore–Penrose pseudo-inverse. The thrust forces, f_1, f_2, f_3, and f_4, and tilting angles, θ_1, θ_2, θ_3, and θ_4 are obtained as follows.

$$\begin{aligned} f_1 &= sign(q_5)\sqrt{q_1^2+q_5^2}, \\ f_2 &= sign(q_6)\sqrt{q_2^2+q_6^2}, \\ f_3 &= sign(q_7)\sqrt{q_3^2+q_7^2}, \\ f_4 &= sign(q_8)\sqrt{q_4^2+q_8^2}, \end{aligned} \tag{9}$$

$$\begin{aligned} \theta_1 &= \arctan\frac{q_1}{q_5}, \theta_2 = \arctan\frac{q_2}{q_6}, \\ \theta_3 &= \arctan\frac{q_3}{q_7}, \theta_4 = \arctan\frac{q_4}{q_8}, \end{aligned} \tag{10}$$

where q_i is the ith component of input q.

3.2. Practical solution using the redundancy

3.2.1. Method for minimization of thrust force

A control algorithm suitable for the tilting mechanism was developed using the redundancy. Thus, we can use **N,** the null-space of vectors **A**, considering that the size of matrix A is 6×8. q is derived as follows.

$$q = \mathbf{A}^+\tau + \mathbf{N}z \tag{11}$$

where $\mathbf{A}^+ = \mathbf{A}^T(\mathbf{A}\mathbf{A}^T)^{-1}$, $\mathbf{N} = (\mathbf{I}_8 - \mathbf{A}^+\mathbf{A})$, and $\mathbf{I}_N$ is the identity matrix of dimension N, and the vector $z \in \Re^8$ in Eq. (11) is an additional free quantity projected onto the null-space of **A**, whose use is detailed in Section 3.2.2. The vector q that minimizes the norm of τ is derived by the pseudo-inverse of **A**, and consequently, the thrust force is minimized.

3.2.2. Method for avoiding bound of tilting angles

As a next step, we discuss how to exploit the additional command z in Eq. (11). z is projected into the null-space of A.

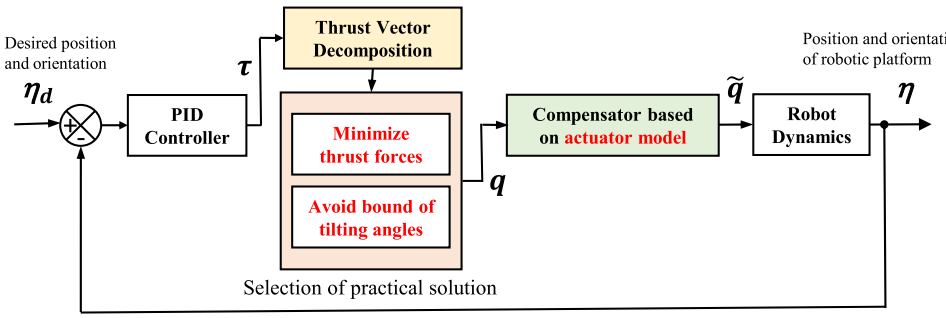

Fig. 6. Diagram of PID controller with decomposition and compensator based on the actuator model (PID-DC controller).

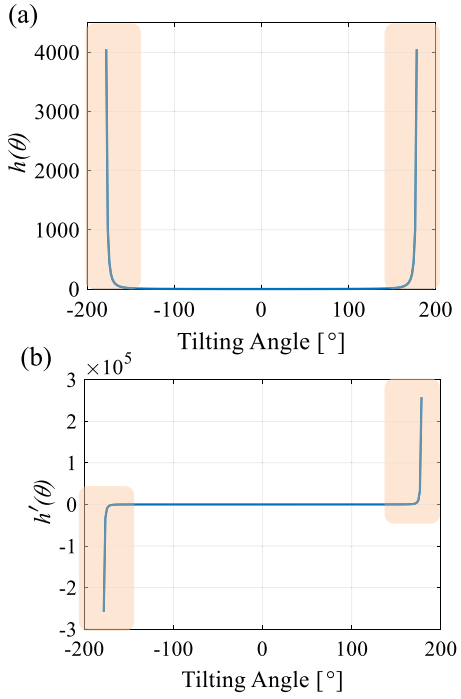

Fig. 7. (a) The function $h(\theta)$ model to avoid the bound of tilting angles. (b) $h'(\theta)$ is the derivative function of $h(\theta)$. θ_b is 180° and γ is 0.5.

Thus, it does not produce any action that would interfere with the targeted thrust force. This means that z can be exploited to fulfill additional tasks without interfering with the original purpose. The result of the previously mentioned calculation is likely to release the tilting angles randomly without considering the actual rotation of the thruster. For example, it is possible to derive a solution in which the tilting angle changes from $-180°$ to $+180°$ repeatedly. If the tilting angle around the boundary is derived alternately, it has a negative effect on the hovering performance of the robot. To find q that reduces the rapid change in the tilting angle while maintaining a minimized thrust force, we propose a new model as follows [25,26].

$$H(\theta) = \sum_{i=1}^{4} h(\theta_i) \tag{12}$$

$h(\theta_i)$ is as follows.

$$h(\theta_i) = \tan 2(\gamma\theta_i) \tag{13}$$

where $|\theta_i| < \theta_b$ and θ_b are the bounds of the tilting angle, and the h function and its partial derivative function are shown in Fig. 7. With θ respect to the bounds, its slope increases rapidly. The minimization of $H(\theta)$ is then obtained by setting z in Eq. (14).

$$z = -k_H \begin{bmatrix} \nabla_\theta H(\theta) \\ \mathbf{0} \end{bmatrix} \tag{14}$$

where k_H is the gain for the new model, and the gradient term of $H(\theta)$ and zero vector are 4×1, respectively.

By applying this function, the tilting angle near the boundary value of the tilting angle was reduced.

3.3. PID controller with a compensator based on the actuator model

This study designed a controller based on PID control. The decomposed control input q with the null-space solution for the tilting angle limit from is derived as follows.

$$q = \mathbf{A}^+ \left[\mathbf{J}^T(\eta) \left(\mathbf{K}_p e + \mathbf{K}_i \int_0^t e(\tau) d\tau - \mathbf{K}_d \dot{\eta} \right) + g(\eta) \right] - k_h \mathbf{N} \begin{bmatrix} \nabla_\theta H(\theta) \\ 0 \end{bmatrix} \tag{15}$$

where η is the position and orientation vector in the earth-fixed frame, and $g(\eta)$ is the gravitational force and buoyant force, and $\mathbf{K}_p$, $\mathbf{K}_i$, and $\mathbf{K}_d$ are the diagonal matrices of proportional, integral, and differential gains, respectively. $\mathbf{K}_p$ = diag(44, 150, 38, 5, 56, 12), $\mathbf{K}_i$ = diag(0.37, 0.72, 0.42, 0.11, 0.18, 0.14), and $\mathbf{K}_d$ = diag(89, 200, 101, 6, 37, 12) are set as the optimal gains, $\mathbf{J}$ is the Jacobian matrix, and k_h is the gain for the null-space projection. The obtained q is converted into tilting angles (θ_1, θ_2, θ_3, θ_4) and thrust forces (f_1, f_2, f_3, f_4) using Eqs. (9) and (10). Thrust forces are converted once more to the angular velocities (Ω_1, Ω_2, Ω_3, Ω_4) of the thruster screw using Eq. (4).

Saturation in actuators is a challenging issue in controller design [27]. Most actuators need to accelerate and decelerate owing to the required torque, motor size, and wear of the rotary seal. Thus, they cannot be driven at infinitely high speeds. In previous studies, the robot was unable to maintain stability in the experiments because of the saturation of the tilting thrusters [17]. The control input can oscillate significantly, but the actual actuator speed of the tilting mechanism could not follow the change. Considering this problem, we designed a compensator that applied the actual model obtained by experiments in water. The compensator considering the models of Eqs. (5) and (6) limits the speed of the control input by avoiding saturation in actuation.

$$\dot{q} = \left(\tilde{q}_{prev} - q\right) / \Delta t, \tag{16}$$

$$\dot{\tilde{q}} = \begin{cases} \dot{q}_b & (\dot{q} > \dot{q}_b) \\ \dot{q} & (-\dot{q}_b \le \dot{q} \le \dot{q}_b) \\ -\dot{q}_b & (\dot{q} < -\dot{q}_b) \end{cases}, \tag{17}$$

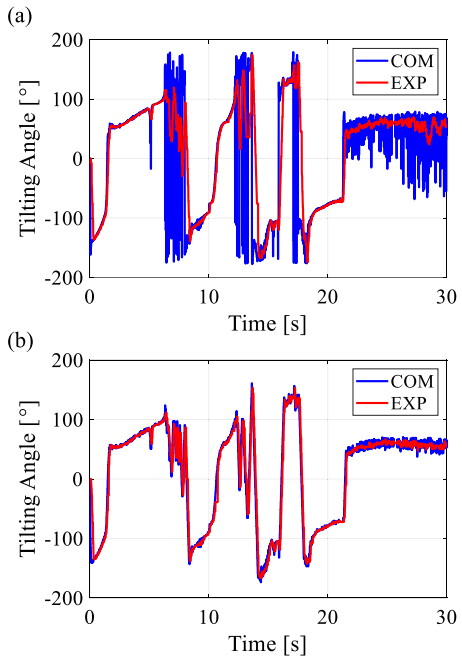

Fig. 8. [Experiment] Tilting angle of a rotating thruster, blue line is the input from controller (a) without compensator, (b) with compensator. The blue line is command (COM) and the red line represents experimental results (EXP). . (For interpretation of the references to color in this figure legend, the reader is referred to the web version of this article.)

$$\tilde{q} = \tilde{q}_{prev} + \dot{\tilde{q}}\Delta t. \tag{18}$$

q is the control input generated by the controller. Both tilting angles and thruster RPM can be substituted for q. $\tilde{q}_{prev}$ is the control input actually entered into the robot in the previous control step, Δt is the control period, and $\dot{q}_b$ is the limit of the speed of actuation. In this study, the control period is 10 ms, the limit of tilting speed of the tilting motor, and angular acceleration of the thruster propeller are 100°/s and 5800 rpm/s, respectively. The speed of each actuator is limited to be derived only within the range of speeds that can actually be followed.

3.4. Stability analysis

In this study, a controller based on PID control is designed. PID control is widely used, and the stability analysis of a typical PID controller has been proved by

The error dynamics of the 6-DOF motion for the desired position and orientation η_d are derived as follows.

$$\mathbf{M}_\eta(\eta)\ddot{e} + \mathbf{C}_\eta(\nu,\eta)\dot{e} + \mathbf{D}_\eta(\nu,\eta)\dot{e} = \mathbf{J}^{-T}(\eta)\tau, \tag{19}$$

where $e := \eta_d - \eta$, $\dot{e} = -\dot{\eta}$, $\ddot{e} = -\ddot{\eta}$. $\mathbf{M}$ is the inertial matrix including the added mass, $\mathbf{C}$ is the matrix of the Coriolis, centripetal, and velocity-dependent terms due to added mass, $\mathbf{D}$ is the damping matrix, which includes drag force terms, and the subscript η indicates the earth-fixed frame. ν is the linear and angular velocity in the body frame. A more detailed description is provided in Appendix A.

Substituting Eqs. (7) and (15) into Eq. (19), the stability condition can be derived as follow:

$$\mathbf{K}_d > \mathbf{M}_\eta, \mathbf{K}_i > 0, \mathbf{K}_p > \mathbf{K}_d + \frac{2}{\alpha}\mathbf{K}_i \tag{20}$$

where α is a small positive constant chosen so small that:

$$\frac{1}{2}(1-\alpha)\mathbf{K}_d - \alpha\mathbf{M}_\eta + \frac{\alpha}{2}\sum_{i=1}^{6}(\eta_i - \eta_{id})\frac{\partial \mathbf{M}_\eta}{\partial \eta_i} > 0. \tag{21}$$

Considering the null-space projection, the inequality about the additional command z in Eq. (22) ensures stability conditionally [28,29].

$$-z^T z \le 0 \tag{22}$$

Eq. (7) is valid regardless of the null-space projection in the control input q. The asymptotical stability of the system is still preserved but the system reaches a different equilibrium state.

In general, the derived controller with a compensator given by Eqs. (16)–(18) is finite gain stable. The stability analysis of a typical feedback controller such as a PID with a compensator can be proved by Kapasouris [30–32]. Every stable system with bounded inputs is BIBO stable because the outputs are always bounded. The system is finite gain stable because in addition to being BIBO stable, there exists a class of "small" inputs for which the system remains linear. Therefore, the controller that is applied to the robot, i.e., the PID-DC controller, is stable, and this system remains finite gain stable in the presence of any disturbance.

4. Simulation

4.1. Verification of the compensator based on the actuator model

Experiments were conducted to demonstrate the effectiveness of the compensator based on an actual model. Fig. 8(a) shows the operation of the tilting thruster without the compensator, and it can be seen that the actual thruster cannot follow the high rotational speed of the tilting thruster from the controller. In the experiment with the compensator, on the other hand, a smooth control input is obtained, and the thruster chases it well. As a result, this verifies the validity of the empirical thruster model and the performance of the compensator applying it.

4.2. Effect of null-space projection term

As mentioned before, a compensator that added an algorithm to avoid the bound of tilting angles was designed. The simulation results showed the difference between applying the null-space projection term (NST) as in Eq. (11) and applying only Eq. (8). The robot moves 0.4 m in the x-direction and $-30°$ in the pitch direction in 10 s, and then -0.2 m in the y direction in 20 s. In this case, Fig. 9 shows that the result of applying the null-space term follows the command marginally better than when the null-space term is not applied. The tilting angle is also shown during the movement of the robot in Fig. 10. The tendency for tilting angles of plus or minus 180° to be derived alternately has been reduced in the red dotted line with NST, and it can be seen that the rapid vibration of the tilting angle is reduced. This simulation verified the effect that the h function helps to reliably control the robot, considering the actual constraints of the tilting thrust. Therefore, these results imply that the hovering performance of the PID-DC controller with NST will be improved in the experiments.

5. Experiment

5.1. Hovering motion control

The robot maintains the hovering motion at a starting point where it is 0 m for the x position, 0 m for the y position, and 0.4 m for the z position, and moves to the specified posture to return to its original state. The robot keeps the pitch angle at

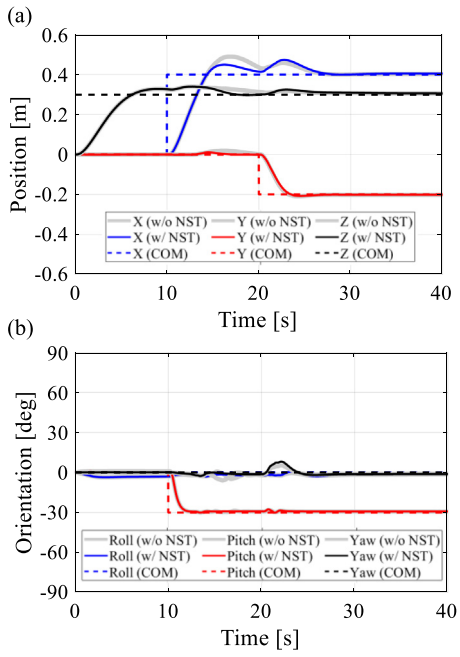

Fig. 9. [Simulation] Hovering control with the null-space projection term (NST); (a) position; (b) orientation. The solid line shows hovering control from the PID-DC with NST compared to the gray thick line, which is the data without NST.

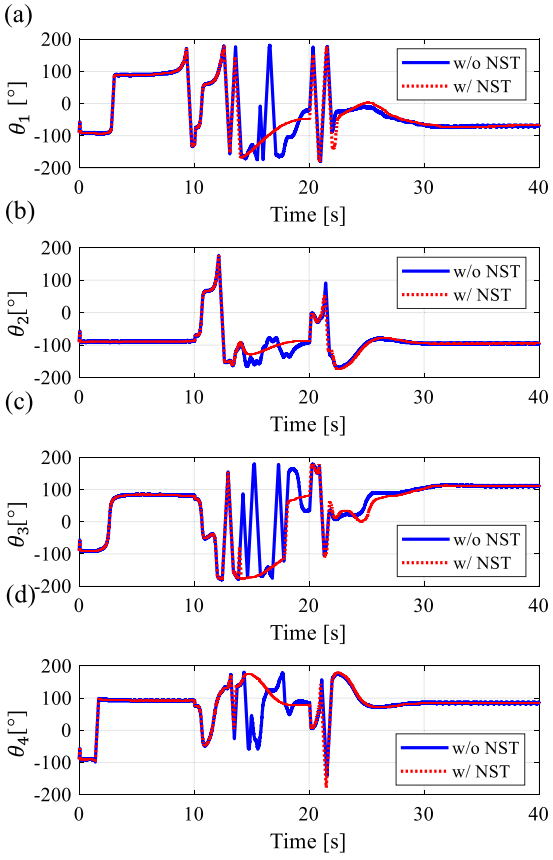

Fig. 10. [Simulation] Tilting angles of thrusters with and without exploiting the null-space term. (a) front left, (b) front right, (c) rear right, (d) rear left.

−30° for 20 s from the start, and then returns to its original position. This posture is selected and tested because it is required to perform various underwater tasks. The results of the position

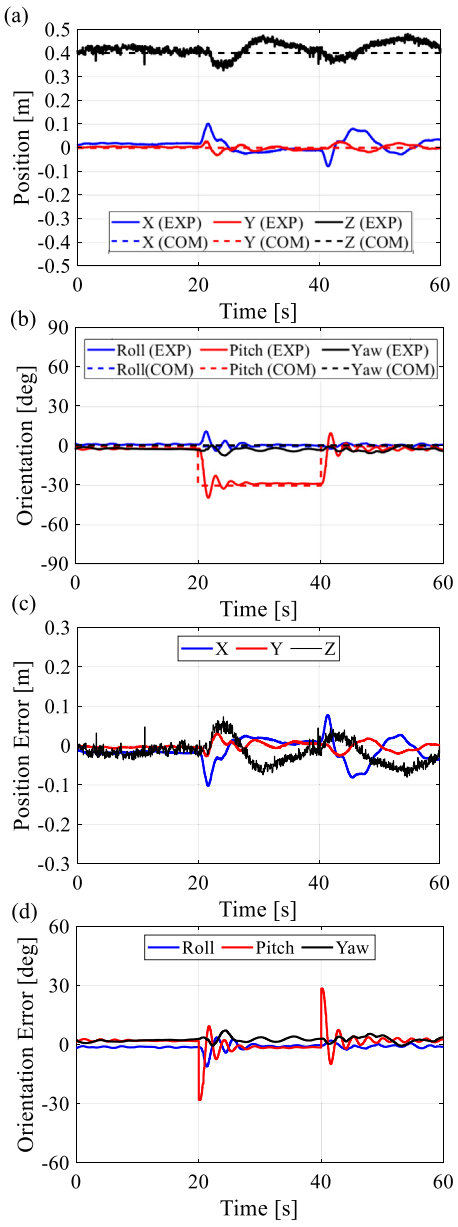

Fig. 11. [Experiment] Hovering with PID-DC controller, (a) position, (b) orientation, (c) position error, (d) orientation error.

and orientation in this experiment are shown in Fig. 11(a) and (b), respectively. The experimental results follow the command relatively well, including a slight overshoot. In the experimental results, the average position root mean square (RMS) error was 0.025 m, the maximum position error was 0.097 m, the average orientation RMS error was 1.2°, and the maximum orientation error was 5.1° during the hovering motion. Figs. 12 and 13 show the tilting angles and thrust forces of each tilting thruster during the hovering experiment, and the tilting propeller follows the compensated control input.

5.2. Hovering motion control

In Fig. 14, the error in the steady state was calculated to compare the stability of the hovering motion of the robot. The error is dimensionless under the assumption that the position errors of 0.01 m and 10° have the same size. Marker I represents

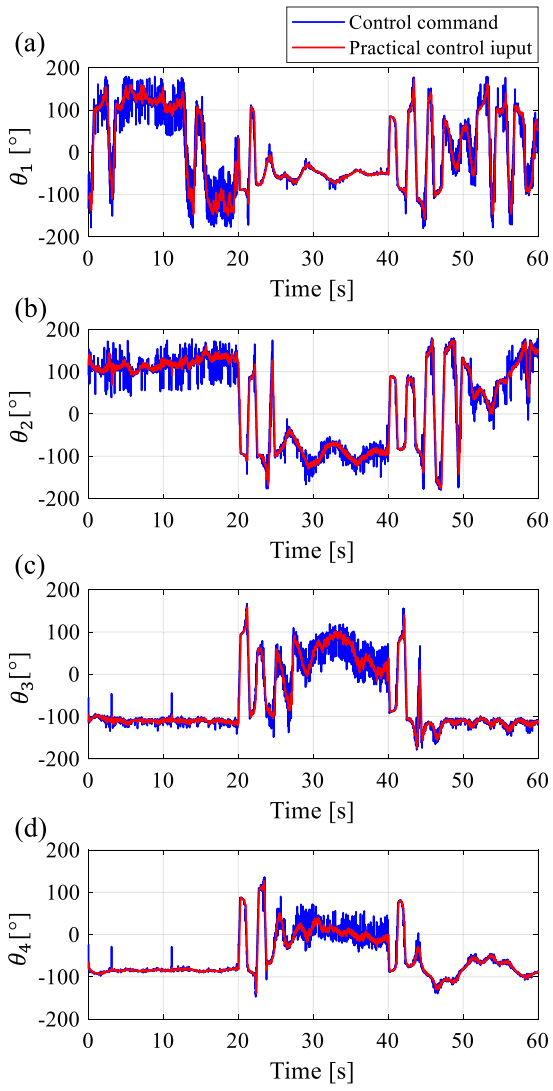

Fig. 12. [Experiment] Tilting angles of tilting thrusters during the hovering motion test.

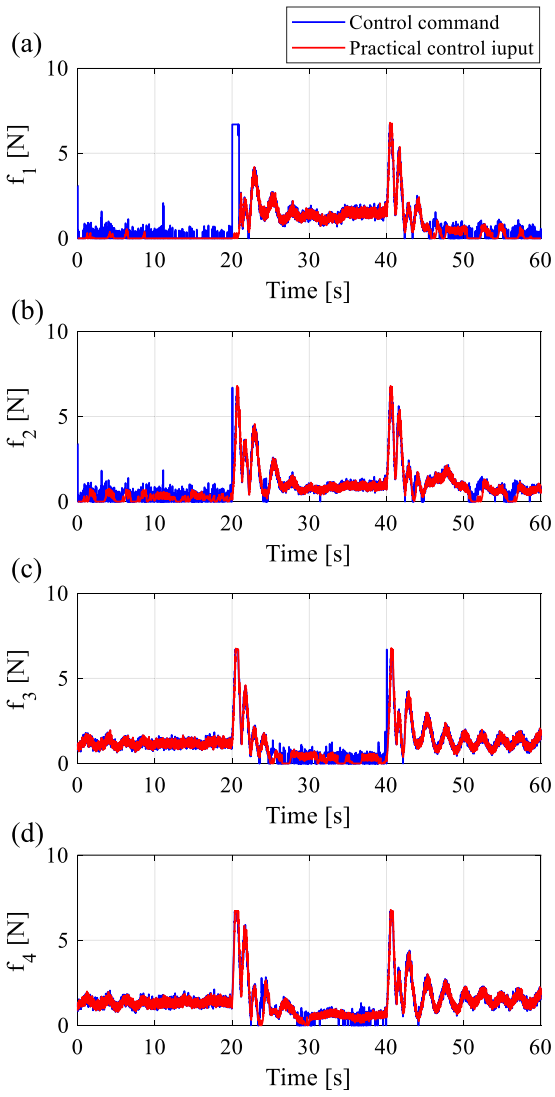

Fig. 13. [Experiment] Thrust forces of tilting thrusters during hovering motion testing.

the deviation of the errors based on the RMS error. It can be seen that the position error, orientation error, and pitch direction error of PID-DC are smaller compared with switching control. These results indicate that the overall performance of the hovering motion, as well as the pitch direction, were improved.

5.3. Hovering motion control with disturbance

A disturbance generator was created using an additional thruster for the disturbance experiment, and the design and manufactured disturbance generator are shown in Fig. 15(a) and (b). The size of the disturbance is determined based on the annual speed of the Cheju Warm Current in Korea from the Kuroshio Current [33,34]. Two environments with disturbances were created in the water tank. In Fig. 15(c), the first case of s is described, which produces a constant force of 3 N for 30 s. The second is a sinusoidal force of approximately 40 s, as shown in Fig. 15(d).

First, the hovering motion test, which maintains a posture of −30° in the pitch direction, was conducted in the first disturbance situation mentioned above. The uncontrolled robot in the water is pushed while a force of 3 N continues to be applied in

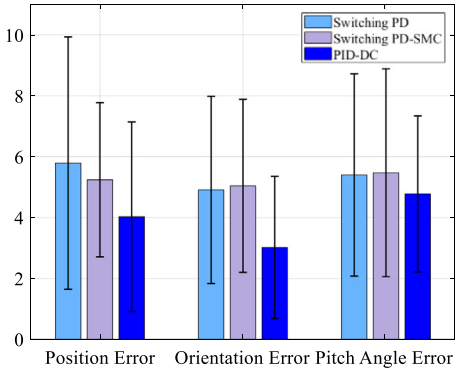

Fig. 14. Comparison of RMS errors with pitch input as −30° in the steady state.

one direction. However, the robot controlled by PID-DC does not move while maintaining the desired posture at a specific position despite external forces. The position and orientation of the robot are shown in Fig. 16(a) and (b), respectively. The error graph in position and orientation was also plotted in Fig. 16(c) and (d). In

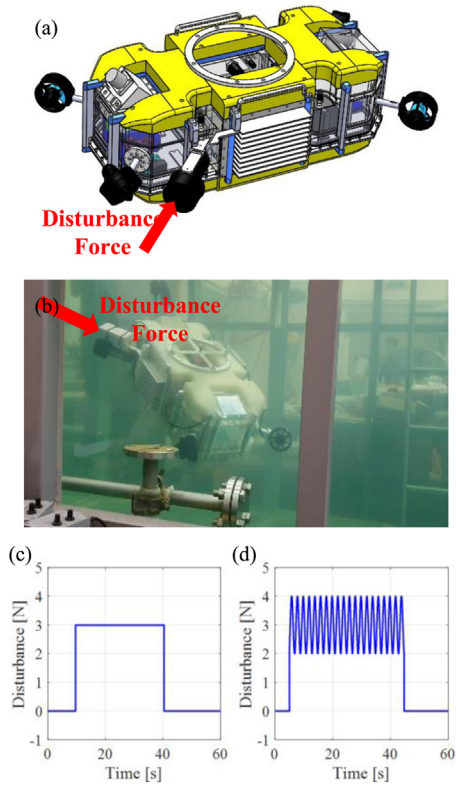

Fig. 15. Disturbance generator of the system. (a) Design of the disturbance generator. (b) Manufactured disturbance generator attached on the robot. (c) Disturbance case 1 is 3 N force for 30 s, (d) Disturbance case 2 is sinusoidal force of 1 N size and 3 N offset for 40 s.

the second case, the robot was disturbed by a sinusoidal force. Similarly, the hovering motion tilted in the pitch direction was tested, and the results are shown in Fig. 16(e)–(h). The results of both cases show that the position and orientation have limited offset and vibration due to the disturbance, but these do not exceed certain bounds. The results of both cases are shown the position and orientation have limited offset and vibration due to the disturbance, but these do not exceed certain bounds. The results of this experiment verify that the robot controlled by PID-DC can keep up 6-DOF hovering motion even when there is a certain disturbance, such as ocean currents.

6. Conclusions

In this paper, a redundant tilting mechanism is presented for an underwater robot with a controller using the decomposition and compensation method based on the actuation model. First, the tilting mechanism was analyzed. Based on this analysis, a redundant tilting mechanism was designed by eliminating the constraints, and the actual model of this mechanism was obtained through experimentation. Second, a new controller suitable for AURORA was proposed by reflecting the model of the actual tilting thruster and finding a practical solution using the redundancy. The nonlinear force input term of the tilting thrusters was decomposed in the horizontal and vertical directions. Based on the pseudo-inverse and null-space projected gradient methods, the solution minimizes the thrust force and avoids the sharp control input in the tilting angles. The final input comes from the compensator, which reflects the model to solve the actuator saturation. Simulations and experiments were performed for the hovering motion of the underwater robot, and the validity of the proposed mechanism and controller was verified through these results. The hovering control performance of the robot was better than that achieved with other switching PD and PD-SMC controls. The robustness of the controller was also demonstrated through disturbance experiments.

Declaration of competing interest

The authors declare that they have no known competing financial interests or personal relationships that could have appeared to influence the work reported in this paper.

Acknowledgments

This work was supported by the International Collaboration Research Program through the National Research Foundation of Korea (NRF) funded by the Ministry of Science and ICT, South Korea (NRF-2017K1A3A1A19071037) and the Department of Science and Technology (DST), India (INT/Korea/P-43).

Appendix A

The matrices in the motion equations of the underwater robot can be derived. $\eta = [x\ y\ z\ \phi\ \theta\ \psi]^{\mathrm{T}}$ denotes the position and orientation vector in the earth-fixed frame and $v = [u\ v\ w\ p\ q\ r]^{\mathrm{T}}$ is the linear and angular velocity in the body frame [14] (Eq. (A.1) is given in Box I).

$$\mathbf{M} = \begin{bmatrix} 96.3 & 0 & 0 & 0 & 0 & 0 \\ 0 & 133.04 & 0 & 0 & 0 & 0 \\ 0 & 0 & 168.57 & 0 & 0 & 0 \\ 0 & 0 & 0 & 4.47 & 0 & 0 \\ 0 & 0 & 0 & 0 & 9.26 & 0 \\ 0 & 0 & 0 & 0 & 0 & 8.1 \end{bmatrix}, \tag{A.2}$$

$$\mathbf{C} = \begin{bmatrix} 0 & 0 & 0 & 0 & 168.57w & -133.04v \\ 0 & 0 & 0 & -168.57w & 0 & 96.30u \\ 0 & 0 & 0 & 133.04v & -96.30u & 0 \\ 0 & 168.57w & -133.04v & 0 & 8.10r & -9.26q \\ -168.57w & 0 & 96.30u & -8.10r & 0 & 4.47p \\ 133.04v & -96.30u & 0 & 9.26q & -4.47p & 0 \end{bmatrix}, \tag{A.3}$$

$$\mathbf{D} = \begin{bmatrix} 34.55\,|u| & 0 & 0 & 0 & 0 & 0 \\ 0 & 104.40\,|v| & 0 & 0 & 0 & 0 \\ 0 & 0 & 146.50\,|w| & 0 & 0 & 0 \\ 0 & 0 & 0 & 0.68\,|p| & 0 & 0 \\ 0 & 0 & 0 & 0 & 5.34\,|q| & 0 \\ 0 & 0 & 0 & 0 & 0 & 3.07\,|r| \end{bmatrix}, \tag{A.4}$$

$$\mathbf{M}_{\eta}(\eta) = \mathbf{J}^{-T}(\eta)\mathbf{M}\mathbf{J}^{-1}(\eta), \tag{A.5}$$

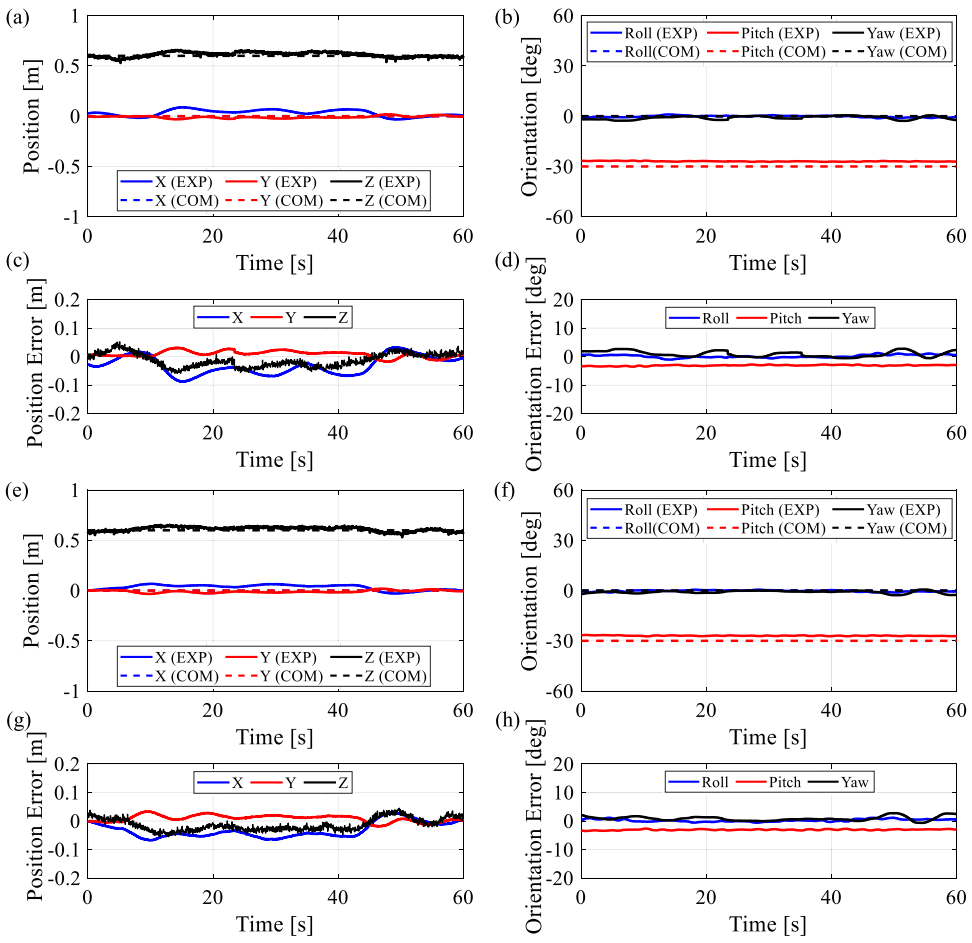

Fig. 16. [Experiment] Hovering motion control tilted in the pitch direction with disturbance. (a) position, (b) orientation, (c) position error, (d) orientation error (case 1), (e) position, (f) orientation, (g) position error, (h) orientation error (case 2).

$$\mathbf{J} = \begin{bmatrix} \cos\psi\cos\theta & -\sin\psi\cos\phi + \cos\psi\sin\theta\sin\phi & \sin\psi\sin\phi + \cos\psi\cos\phi\sin\theta & 0 & 0 & 0 \\ \sin\psi\cos\theta & \cos\psi\cos\phi + \sin\phi\sin\theta\sin\psi & -\cos\psi\sin\phi + \sin\theta\sin\psi\cos\phi & 0 & 0 & 0 \\ -\sin\theta & \cos\theta\sin\phi & \cos\theta\cos\phi & 0 & 0 & 0 \\ 0 & 0 & 0 & 1 & \sin\phi\tan\theta & \cos\phi\tan\theta \\ 0 & 0 & 0 & 0 & \cos\phi & -\sin\phi \\ 0 & 0 & 0 & 0 & \dfrac{\sin\phi}{\cos\theta} & \dfrac{\cos\phi}{\cos\theta} \end{bmatrix}, \tag{A.1}$$

Box I.

$$\mathbf{C}_\eta(\upsilon,\eta) = \mathbf{J}^{-T}(\eta)[\mathbf{C}(\upsilon) - \mathbf{M}\mathbf{J}^{-1}(\eta)\dot{\mathbf{J}}(\eta)]\mathbf{J}^{-1}(\eta), \tag{A.6}$$

$$\mathbf{D}_\eta(\upsilon,\eta)\dot{\eta} = \mathbf{J}^{-T}(\eta)\mathbf{D}(\upsilon)\mathbf{J}^{-1}(\eta). \tag{A.7}$$

Appendix B. Supplementary data

Supplementary material related to this article can be found online at https://doi.org/10.1016/j.robot.2021.103995.

References

[1] J. Yuh, Design and control of autonomous underwater robots: A survey, Auton. Robots 8 (1) (2000) 7–24.
[2] J.G. Bellingham, C.A. Goudey, T.R. Consi, J.W. Bales, D.K. Atwood, J.J. Leonard, C. Chryssostomidis, A second generation survey AUV, in: Proceedings of IEEE Symposium on Autonomous Underwater Vehicle Technology (AUV'94), 1995, pp. 148–155.
[3] K.D. Do, Robust adaptive tracking control of underactuated ODINs under stochastic sea loads, Robot. Auton. Syst. 72 (2015) 152–163.
[4] D. Ribas, N. Palomeras, P. Ridao, M. Carreras, A. Mallios, Girona 500 AUV: From survey to intervention, IEEE/ASME Trans. Mechatronics 17 (1) (2011) 46–53.

[5] I. Torres, J. Torres, R. Lozano, A new AUV configuration with four tilting thrusters: Navigation and hover tasks, in: 2012 9th International Conference on Electrical Engineering, Computing Science and Automatic Control, 2012, pp. 1–6.
[6] B. Xin, L. Xiaohui, S. Zhaocun, Z. Yuquan, A vectored water jet propulsion method for autonomous underwater vehicles, Ocean Eng. 74 (2013) 133–140.
[7] L. Geng, Y. Lin, Z. Hu, C. Wang, L. Meng, D. Li, A new concept spherical underwater robot propelled by thrust vector synthetic jet actuator, in: OCEANS 2016-Shanghai, 2016, pp. 1–4.
[8] S. Desset, R. Damus, F. Hover, J. Morash, V. Polidoro, Closer to deep underwater science with ODYSSEY IV class hovering autonomous underwater vehicle (HAUV), Eur. Oceans 2 (2005) 758–762.
[9] S. Ishibashi, H. Yoshida, T. Hyakudome, M. Sugesawa, T. Nakatani, Y. Ota, et al., The development of an autonomous underwater vehicle Otohime with the multiple operation, in: IEEE International Conference on Mechatronics and Automation, 2013, pp. 1588–1593.
[10] D.J. Lindsay, H. Yoshida, T. Uemura, H. Yamamoto, S. Ishibashi, J. Nishikawa, et al., The untethered remotely operated vehicle PICASSO-1 and its deployment from chartered dive vessels for deep sea surveys off Okinawa, Japan, and Osprey Reef, Coral Sea, Australia, Mar. Technol. Soc. J. 46 (4) (2012) 20–32.
[11] S. Araki, K. Ishii, Development of glider type small AUV Seabird, in: Symposium on Underwater Technology and Workshop on Scientific Use of Submarine Cables and Related Technologies, 2017, pp. 320–325.
[12] A. Jebelli, Design of an Autonomous Underwater Vehicle with Vision Capabilities (Doctoral dissertation), University of Ottawa, 2016.
[13] Y. Li, S. Guo, Y. Wang, Design and characteristics evaluation of a novel spherical underwater robot, Robot. Auton. Syst. 94 (2017) 61–74.
[14] S. Jin, J. Kim, J. Kim, T. Seo, Six-degree-of-freedom hovering control of an underwater robotic platform with four tilting thrusters via selective switching control, IEEE/ASME Trans. Mechatronics 20 (5) (2015) 2370–2378.
[15] J. Bae, J. Bak, S. Jin, T. Seo, J. Kim, Optimal configuration and parametric design of an underwater vehicle manipulator system for a valve task, Mech. Mach. Theory 123 (2018) 76–88.
[16] S. Jin, J. Kim, J. Bae, T. Seo, J. Kim, Design, modeling and optimization of an underwater manipulator with four-bar mechanism and compliant linkage, J. Mech. Sci. Technol. 30 (9) (2016) 4337–4343.
[17] S. Jin, J. Kim, J.W. Kim, J. Bae, J. Bak, J. Kim, T. Seo, Back-stepping control design for an underwater robot with tilting thrusters, in: International Conference on Advanced Robotics (ICAR), IEEE, 2015, pp. 1–8.
[18] J. Bak, H.N. Nguyen, S. Park, D. Lee, T. Seo, S. Jin, J. Kim, Positioning control of an underwater robot with tilting thrusters via decomposition of thrust vector, Int. J. Control Autom. Syst. 15 (5) (2017) 2283–2291.
[19] S. Jin, J. Bak, J. Kim, T. Seo, H.S. Kim, Switching PD-based sliding mode control for hovering of a tilting-thruster underwater robot, PLoS One 13 (3) (2018).
[20] E.P. Cox, A method of assigning numerical and percentage values to the degree of roundness of sand grains, J. Paleontol. 1 (3) (1927) 179–183.
[21] T.I. Fossen, Guidance and Control of Ocean Vehicles, Wiley, New York, 1994.
[22] S. Jin, J. Kim, S. Lee, J. Kim, T. Seo, Empirical modeling of rotating thruster for underwater robotic platform, J. Mar. Sci. Technol. 20 (1) (2015) 118–126.
[23] S. Bennett, Development of the PID controller, IEEE Control Syst. Mag. 13 (6) (1993) 58–62.
[24] D.E. Rivera, M. Morari, S. Skogestad, Internal model control: PID controller design, Ind. Eng. Chem. Process Des. Dev. 25 (1) (1986) 252–265.
[25] B. Nemec, L. Zlajpah, Null space velocity control with dynamically consistent pseudo-inverse, Robotica 18 (5) (2000) 513–518.
[26] M. Ryll, H.H. Bülthoff, P.R. Giordano, Modeling and control of a quadrotor UAV with tilting propellers, in: 2012 IEEE International Conference on Robotics and Automation, IEEE, 2012, pp. 4606–4613.
[27] P. Sarhadi, A.R. Noei, A. Khosravi, Model reference adaptive PID control with anti-windup compensator for an autonomous underwater vehicle, Robot. Auton. Syst. 83 (2016) 87–93.
[28] C. Ott, A. Kugi, Y. Nakamura, Resolving the problem of non-integrability of nullspace velocities for compliance control of redundant manipulators by using semi-definite Lyapunov functions, in: IEEE International Conference on Robotics and Automation(ICRA), 2008, pp. 1999–2004.
[29] H. Sadeghian, L. Villani, M. Keshmiri, B. Siciliano, Task space control of robot manipulators with null space compliance, IEEE Trans. Robot. 30 (2) (2014) 493–506.
[30] P. Kapasouris, Design for Performance Enhancement in Feedback Control Systems with Multiple Saturating Nonlinearities (Doctoral dissertation), Massachusetts Institute of Technology, 1988.
[31] P. Kapasouris, M. Athans, G. Stein, Design of feedback control systems for stable plants with saturating actuators, 1988.
[32] J. Bak, J. Kim, T. Seo, S. Jin, Gain optimization of a controller with decomposition of thrust force and actuation limit algorithm for a tilted thrusting underwater robot, J. Korean Soc. Precis. Eng. 36 (11) (2019) 1025–1031.
[33] M.G. Gross, Oceanography, sixth ed., Merrill, Columbus, 1990, pp. 74–75.
[34] H.J. Lie, C.H. Cho, J.H. Lee, S. Lee, Y. Tang, Seasonal variation of the Cheju warm current in the northern East China Sea, J. Oceanogr. 56 (2) (2000) 197–211.

Jeongae Bak received her B.S. degree in 2014 from the School of Mechanical Engineering, Hanyang University, Seoul, Korea, and a Ph.D. in 2020 from the School of Mechanical and Aerospace Engineering, Seoul National University, Seoul, Korea. She is currently a Senior Researcher with Department of Robotics & Mechatronics at Korea institute of machinery and materials. Daejeon, Korea. Her current research interests include underwater robotic platform design and control.

Yecheol Moon received his B.S. degree from the Division of Mechanical Engineering and a Master's degree in 2020 from the Department of Mechanical Convergence Engineering at Hanyang University, Korea. He studied a torque redistribution algorithm in underwater parallel manipulator operation by using robust design method. His current research interests include manipulator mechanical design and manipulator control.

Jongwon Kim is Professor at the School of Mechanical and Aerospace Engineering, Seoul National University, Korea. He received a B.S. degree from Seoul National University (SNU) in 1978, an M.S. degree from KAIST, Korea, in 1980, and a Ph.D. from the University of Wisconsin–Madison in 1987, all in mechanical engineering. From 1980 to 1989, he worked with the Division of Machine Tools at Daewoo Heavy Industries (now Doosan Infracore). He is currently a coordinator of the Robotics@SNU group. His current research interests include parallel mechanism machines, Taguchi methods, and robotic platform design. He was Director of the Intelligent Robotics Research Institute and the Institute of Advanced Machines and Design at SNU. He is currently Director of the ProCEED Idea Factory at SNU. His work on parallel mechanism machine tools and robots has been recognized with the Best Paper Award from the ASME Manufacturing Engineering Division, the Society of Manufacturing Engineers (SME) University LEAD Award, and the Outstanding Research Award from the Korean Society of Precision Engineers. He has also received several teaching excellence awards from the University, the SNU College of Engineering, and the Korean Society for Engineering Education.

Santhakumar Mohan received his Ph.D. in 2010 from Robotics and Control from IIT Madras, Chennai, India. He is currently Associate Professor with the Department of Mechanical Engineering, IIT Palakkad, Palakkad, India. His current research interests include underwater vehicle and underwater manipulator design and control, parallel robotic platforms, assistive robots, field and service robots, intelligent motion control, and dynamic modeling and control of dynamic systems. Dr. Mohan was a recipient of the Outstanding Young Scientist for the year 2014 from the Korea Robotics Society, the European Master on Advanced Robotics Plus (EMARO+) fellowship from 2018 to 2019, and the Alexander von Humboldt (AvH) Fellowship from 2016 to 2017.

Tae Won Seo received his B.S. and Ph.D. degrees in 2003 and 2008, respectively, from the School of Mechanical and Aerospace Engineering from Seoul National University, Seoul, Korea. He is currently Associate Professor with the School of Mechanical Engineering, Hanyang University, Seoul, Korea. Before Hanyang University, he was a Postdoctoral Researcher at the Nanorobotics Laboratory, Carnegie Mellon University, visiting Professor at Biomimetic Millisystems Laboratory, UC Berkeley, and an Associate Professor at the School of Mechanical Engineering, Yeungnam University, Korea. His research interests include robot design, analysis, control, optimization, and planning. Dr. Seo was the recipient of the Best Paper Award of the IEEE/American Society of Mechanical Engineers (ASME) Transaction on Mechatronics in 2014, and is currently working as a Technical Editor of IEEE/ASME Transactions on Mechatronics, Associate Editor of IEEE Robotics and Automation Letters, and Intelligent Service Robots.

Sangrok Jin received his B.S. degree in 2008 and PhD in 2014 from the School of Mechanical and Aerospace Engineering, Seoul National University, Seoul, Korea. He was Postdoctoral Researcher at Seoul National University from 2014 to 2016. From 2016 to 2017, he was Senior Research Associate at the University of Texas Health Science Center, Houston, TX, USA. Since 2017, he has been Assistant Professor at the Pusan National University, Busan, Korea. His research interests include the design and control of robotic systems.